Advances in Technology Innovation, vol. 11, no. 4, 2026, pp. 500-520

Mechanistic Influence of Wheelset Bracket Orientation on Load Transfer and Structural Efficiency of Railway Bogie Frames Using FEM

Ryan Olivianto[1], Achmad Fauzan Hery Soegiharto[1,*], Mohamad Irkham Mamungkas[1], Tim Pasang[2], Abi Mufid Octavio[1]

[1]Department of Mechanical Engineering, University of Muhammadiyah Malang, Malang, Indonesia

[2]Department of Engineering Design, Manufacturing, and Management Systems, Western Michigan University, Kalamazoo, United States

Received 12 March 2026; received in revised form 19 May 2026; accepted 21 May 2026

DOI: https://doi.org/10.46604/aiti.2026.16257

Abstract

This study investigates the influence of wheelset bracket orientation on the load transfer mechanism and structural performance of railway bogie frames using finite element analysis. Three configurations, namely vertical, horizontal, and cross orientations, were modeled and evaluated in ANSYS Workbench under identical material properties, boundary conditions, and loading scenarios. Static, dynamic, and impact loading conditions were considered to assess stress, deformation, and structural safety. The results show that bracket orientation significantly affects load distribution and structural response. Among the investigated configurations, the horizontal orientation exhibits the most favorable performance, characterized by lower stress concentration, reduced deformation, higher stiffness, and improved safety margins. In contrast, the vertical orientation demonstrates the most critical response and operates closer to the material yield limit. These findings confirm that wheelset bracket orientation is an important design parameter influencing the reliability, durability, and structural efficiency of railway bogie frames.

Keywords: finite element analysis, railway bogie frame, wheelset bracket orientation, structural response

1. Introduction

The railway industry is a strategic sector in the modern transportation system that demands high levels of safety, reliability, and structural efficiency [1]. In operational practice, railway systems face complex static and dynamic loads due to vehicle weight, inertial forces during acceleration and braking, and track irregularities [2]. These conditions require each structural component to work reliably in distributing loads and maintaining vehicle stability during service [3].

One of the structural problems often encountered in the field is the occurrence of stress concentration in the bogie frame. This issue is especially prominent in the area of load-bearing component joints, where local deformation tends to occur [4]. The bogie frame distributes loads from the train body to the wheels and rails while maintaining safety, stability, and ride comfort [5]. Therefore, the bogie frame must ensure sufficient strength, rigidity, and efficient load distribution to minimize adverse mechanical responses [6].

In the bogie system, the wheelset bracket is a key component that functions as a connector between the wheel axle and the bogie frame [7]. This component receives vertical loads from the vehicle weight as well as significant lateral and longitudinal forces, especially during braking and on curved tracks [8]. Geometrically, the orientation of the wheelset bracket

* Corresponding author. E mail address: achmadfauzan@umm.ac.id

has the potential to affect the load transfer path, stiffness redistribution, and stress concentration patterns on the bogie frame [9]. However, in conventional design practices, the orientation of the wheelset bracket is generally determined based on geometric and manufacturing considerations. It is often treated as a secondary design detail without in-depth structural evaluation [10].

With advances in computational technology, finite element analysis (FEA) is widely used to evaluate the structural response of bogie frames and their components. Various studies have utilized FEA to analyze stress distribution, deformation, and structural response to operational loading [11]. Some studies have even combined FEA with multibody dynamics to evaluate the fatigue response of bogie frames under cyclic loading, thereby identifying critical areas prone to material failure [12]. However, these studies generally focus on dynamic and fatigue responses. Comparative static analysis of geometric orientation variations in the wheelset bracket has not been a major concern. In addition, FEA-based static analysis of bogie frames is also widely used as a verification tool to assess design feasibility against specific criteria and standards [13]. The results of these studies generally show that the bogie frame design is within the acceptable deformation and stress limits based on the properties of the materials used [14]. This approach effectively meets the minimum structural safety requirements under static loading conditions. However, these analyses are generally verifiable and are only performed on one wheelset bracket configuration that represents the existing design.

In addition, several studies report that structural components made of repetitive elements, such as brackets and supporting frames, can behave like periodic structures. This similarity influences their overall mechanical response. In such systems, geometric arrangement strongly influences stiffness distribution and load transfer direction. Even small geometric variations can affect stress concentration and strain energy distribution [15].

Finite element analysis has also been widely applied to investigate both linear and nonlinear structural responses in engineering systems. Nonlinear behavior may arise from material properties or geometric effects, as reported in previous finite element studies on shell and structural systems [16]. In this context, the equivalent stress criterion is commonly used to evaluate the equivalent stress under multiaxial loading and to assess the structural response in a consistent manner [17]. These findings show that geometric configuration should not be treated as a secondary design factor. It significantly affects load transfer and overall structural response, especially where stiffness distribution and force flow are critical.

In general, previous studies have focused on a single wheelset bracket configuration. They have not compared how variations in geometric orientation affect the structural response of bogie frames. Variations in wheelset bracket orientation have generally not been treated as a major structural variable in bogie frame analysis. This is because existing studies are more oriented towards design feasibility verification rather than understanding the mechanisms of load transfer and structural stiffness redistribution. As a result, the available data is still limited in quantitatively explaining the influence of the geometric orientation of the wheelset bracket. Bracket orientation effects on deformation, stress concentration, and strain energy in bogie frames remain insufficiently studied.

To date, research systematically comparing several wheelset bracket orientations remains relatively limited. Most studies only evaluate one configuration in a particular numerical modeling scheme. Differences in geometry, materials, boundary conditions, and loading hinder direct comparisons between orientations. Thus, the isolated effect of wheelset bracket orientation remains unclear under controlled conditions.

Therefore, the influence of wheelset bracket orientation on the load transfer mechanism and structural efficiency of bogie frames has not been systematically investigated. Although many studies have applied FEA to assess the deformation, stress, and structural safety of bogie components, most have examined only a single design case. These studies mainly assess feasibility and strength, leaving the effect of wheelset bracket orientation insufficiently addressed. This limitation is especially relevant when all configurations are assessed under consistent modeling assumptions.

Previous studies mainly evaluate a single wheelset bracket configuration. These studies focus on design feasibility and strength verification. As a result, the influence of bracket orientation is not clearly identified. Differences in geometry, material properties, boundary conditions, and loading between studies make direct comparison difficult. Therefore, the effect of bracket orientation as an independent variable remains unclear. This study addresses this gap by comparing three bracket orientations: vertical, horizontal, and cross. All configurations use the same material properties, boundary conditions, and loading scheme. The only variable considered in this study is the geometric orientation of the wheelset bracket. This approach allows a direct comparison of deformation, stress distribution, strain, and strain energy to evaluate the influence of bracket orientation.

This study presents a systematic evaluation of wheelset bracket orientation as a key geometric parameter influencing structural response in bogie frames. Unlike previous studies that typically focus on a single configuration, this work provides a direct comparison of multiple orientations under identical modeling conditions. The main contribution of this study is a controlled comparison of three bracket orientations under identical modeling conditions. This approach isolates geometric orientation effects on load transfer and structural response. This contribution is particularly important for improving structural reliability and reducing maintenance requirements in railway vehicle systems.

From a practical perspective, the findings provide direct guidance for the design and optimization of bogie frame structures in railway applications. The identification of an optimal bracket orientation can reduce stress concentration and improve load distribution, which are critical factors for structural durability and service life. This is particularly relevant for real-world railway systems. Repeated dynamic and impact loading conditions can significantly affect structural integrity. Therefore, the results of this study can support more reliable and efficient design strategies in engineering practice.

2. Finite Element Analysis

In this research, the finite element method (FEM) was used to evaluate the static structural response of a railway bogie frame under controlled loading conditions [18].

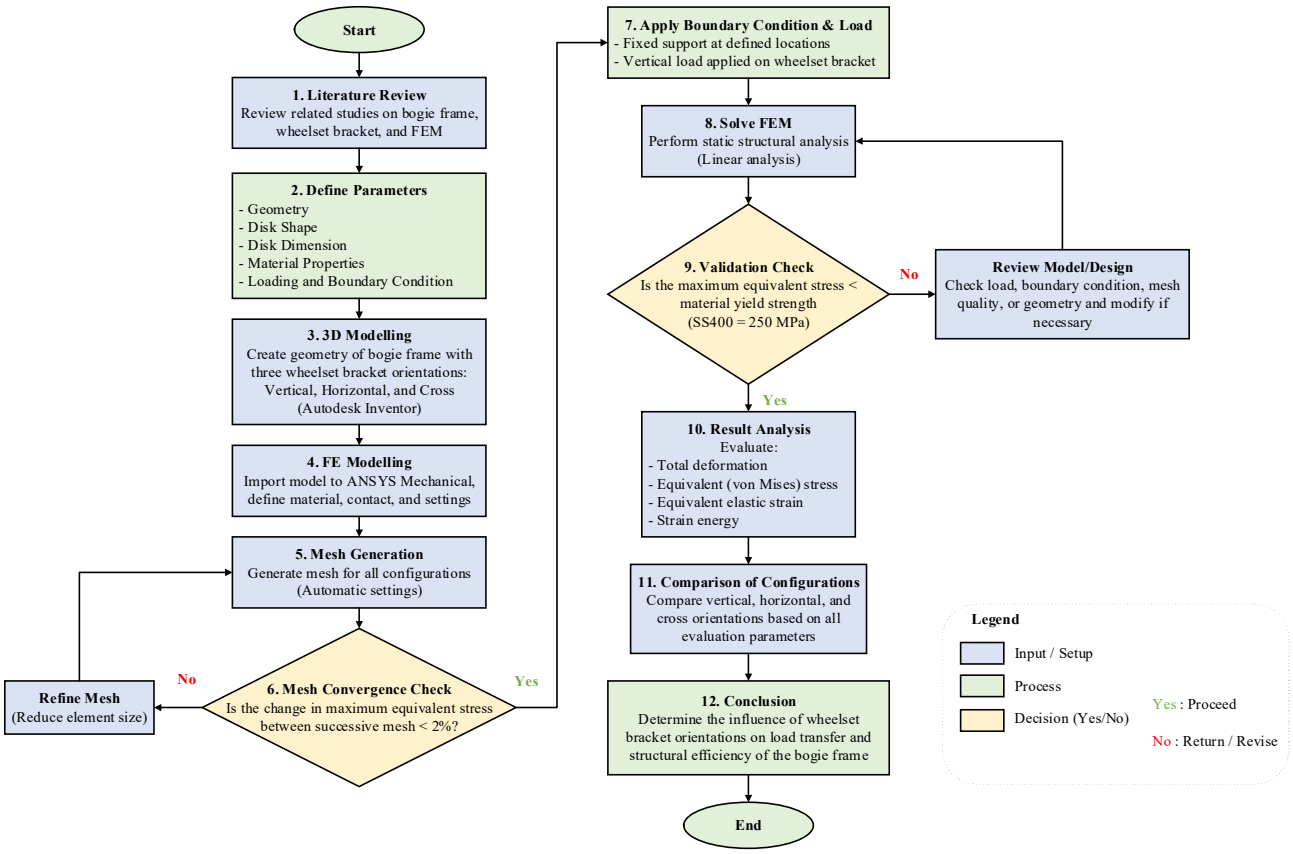

Fig. 1 Research flowchart

The analysis was performed using the Static Structural module in ANSYS Workbench software. This module allows quantitative evaluation of deformation, stress distribution, elastic strain, and strain energy in structural components due to static loading. The main variable examined in this study is the geometric orientation of the wheelset bracket. Three configurations, vertical, horizontal, and cross, were analyzed using identical numerical modeling conditions to enable direct comparison. The overall research procedure adopted in this study is illustrated in Fig. 1, which outlines the sequential steps from geometric modeling to numerical simulation and result evaluation.

2.1. Geometric Model and Wheelset Bracket Configuration

A three-dimensional bogie frame model was developed to represent the primary load-bearing structure of a railway bogie system. Geometric modeling was performed by maintaining the main dimensions of the frame, the thickness of structural elements, and the arrangement of main beams and braces [19]. This approach aims to adequately represent the force flow path and structural stiffness characteristics. This modeling strategy enables a relevant simulation of bogie frame behavior under static loading.

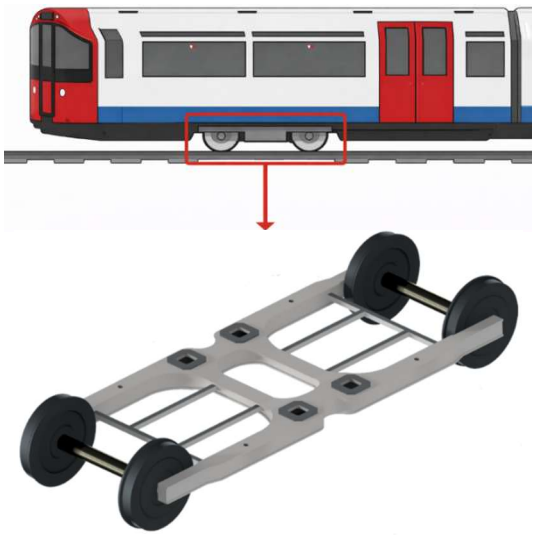

Fig. 2 Train Bogie

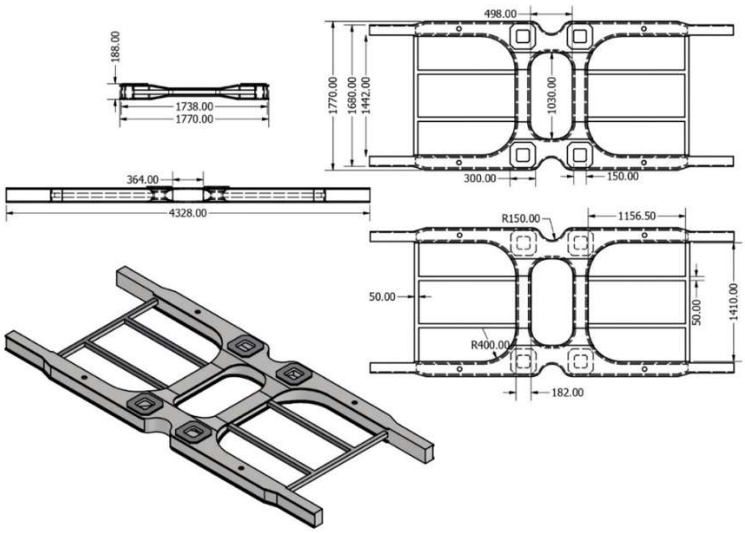

Fig. 3 Bogie Geometry

Design variations in this study are limited to the wheelset bracket configuration as the load transfer interface. Three bracket orientations, namely vertical, horizontal, and cross, are analyzed with equivalent dimensions and mounting positions. All other structural features are kept identical to ensure a consistent modeling framework. The configurations are defined based on simplified load transfer directions. The vertical configuration represents a load path aligned with the main structure. The horizontal configuration represents a perpendicular load path. The cross configuration combines both orientations. These configurations are treated as idealized cases to allow the influence of geometric orientation to be evaluated under controlled conditions. The configurations analyzed in this study are shown in Figs. 2, 3, and 4, respectively.

(a) Vertical wheelset bracket (b) Horizontal wheelset bracket (c) Cross wheelset bracket

Fig. 4 Configuration wheelset bracket design

2.2. Material Properties

The bogie frame and wheelset bracket materials were modeled as isotropic linear elastic materials to maintain consistency and comparability between configurations [20]. The material properties used in this study represent structural steel commonly applied to railway components, specifically SS400 [21]. Thus, the mechanical response of the simulation remains representative of structural behavior under the applied loading conditions.

In this study, SS400 structural steel with an elastic modulus of 2×10^5 MPa, a Poisson's ratio of 0.3, and a density of 7850 kg/m³ was used. The stress-strain relationship of SS400 structural steel is illustrated in Fig. 5, showing linear elastic behavior up to the yield strength of approximately 250 MPa. The complete material properties used in the simulation are summarized in Table 1. The yield stress and maximum tensile stress values were used as references for interpreting the equivalent stress results [22].

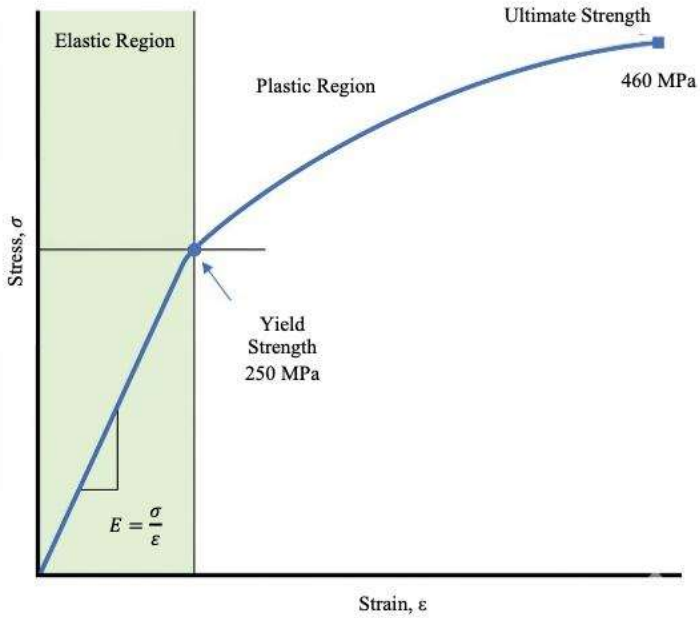

Fig. 5 Stress-strain curve of SS400 structural steel

Table 1 Material properties

Material Properties	Value
Young's Modulus (E)	2e+05 MPa
Poisson Ratio (ν)	0.3
Bulk Modulus	1.6667e+05 MPa
Shear Modulus	76923 MPa
Density (ρ)	7850 kg/m³
Compressive Yield Strength	250 MPa
Ultimate Strength	460 MPa
Yield Strength	250 MPa

2.3. Finite Element Modeling

The model uses 3D quadratic tetrahedral elements (TET10). Each node has three translational degrees of freedom. These correspond to displacement in the x, y, and z directions. Quadratic elements improve accuracy in capturing stress gradients. This is especially important in regions with complex geometry. Mesh refinement is applied near the wheelset bracket. A coarser mesh is used in non-critical regions to reduce computational cost [23]. As shown in Fig. 6, mesh refinement is applied in critical regions near the wheelset bracket connection to capture stress concentration accurately.

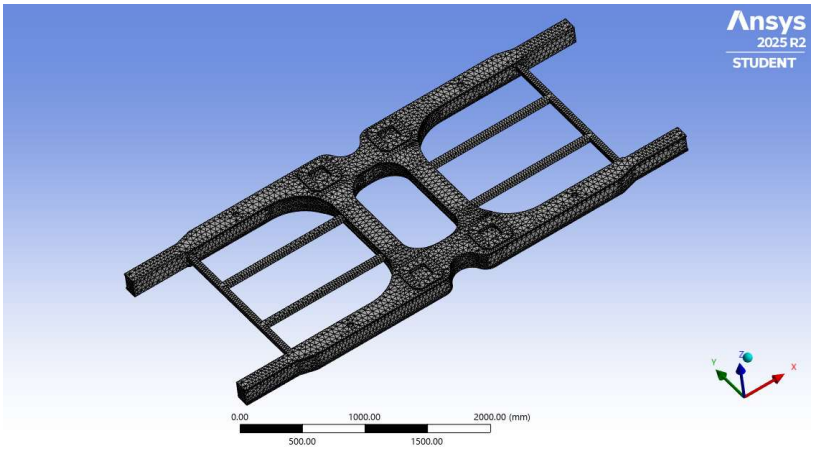

Fig. 6 Meshing

A mesh convergence study was performed to evaluate the influence of mesh density on the numerical results. The relative error of the maximum equivalent stress is calculated by

$$\text{Relative Error} = \frac{|\sigma_i - \sigma_{ref}|}{\sigma_{ref}} \times 100\% \tag{1}$$

Where σ_i is the equivalent stress obtained from each mesh configuration, and σ_{ref} is the reference stress corresponding to the finest mesh. The results of the mesh convergence study are summarized in Table 2, showing the variation of equivalent stress and relative error for different mesh sizes.

Table 2 Mesh convergence study based on equivalent stress

Mesh Size (mm)	Number of Elements	Equivalent Stress (MPa)	Relative Error (%)
20	62988	168.854	0
21	55325	166.914	1.15
22	54136	168.642	0.13
23	49529	168.945	0.05
24	45567	166.845	1.19
25	42935	167.860	0.59
26	41741	166.489	1.40

The convergence results indicate that the variation in equivalent stress is less than 1.40%, with most values below 1%. This demonstrates that the numerical solution has reached mesh independence. Among the tested configurations, the mesh size of 23 mm exhibits the smallest deviation of 0.05% compared to the reference solution. This indicates that further mesh refinement does not significantly affect the results. Therefore, the mesh size of 23 mm was selected as the optimal configuration, as it provides a suitable balance between computational efficiency and numerical accuracy.

Accordingly, this selected mesh configuration was adopted for the final finite element model. The final mesh consists of 50,143 elements and 101,200 nodes, including 17,195 corner nodes and 84,005 mid-side nodes, confirming the use of quadratic tetrahedral elements. This mesh density ensures an adequate balance between computational efficiency and solution accuracy. To ensure the reliability of the finite element model, a validation assessment was conducted based on numerical consistency, material limits, and structural response behavior. The accuracy of the finite element model was evaluated based on mesh convergence and consistency with material limits. The maximum equivalent stress remains below the yield strength of SS400 steel (250 MPa), confirming elastic behavior. Deformation distribution is physically consistent, with maxima at high-load and geometric discontinuity regions.

The mesh convergence study shows that the variation in equivalent stress is less than 1.40%, indicating that the discretization error is minimal. Therefore, the model is considered sufficiently accurate for comparative structural analysis. This approach is consistent with previous studies, where mesh convergence is used as a primary criterion to ensure the accuracy of finite element results [24]. Model validation based on consistency with material behavior and structural response is also widely adopted in finite element analysis [25].

2.4. Boundary Conditions and Loading

Boundary conditions are applied to represent the static working conditions of the bogie frame. The weight of the train car is 20,000 kg. Four concentrated vertical loads are applied at the wheelset bracket locations, each with a magnitude of 24.525 kN, resulting in a total applied load of approximately 98.1 kN. These loads are directed downward to simulate the vertical force transmitted from the wheels during operation.

In addition to external loading, gravitational acceleration of 9.81 m/s² was included to account for the self-weight of the structure. The support conditions were modeled using remote displacement constraints applied at four boundary regions of the frame. All translational degrees of freedom (Ux, Uy, Uz) at these regions were restricted to simulate fixed support conditions. Rotational degrees of freedom were inherently constrained due to the use of solid elements. Boundary conditions and loading configurations are illustrated in Fig. 7, showing the fixed supports at mounting points and vertical loads at wheelset brackets.

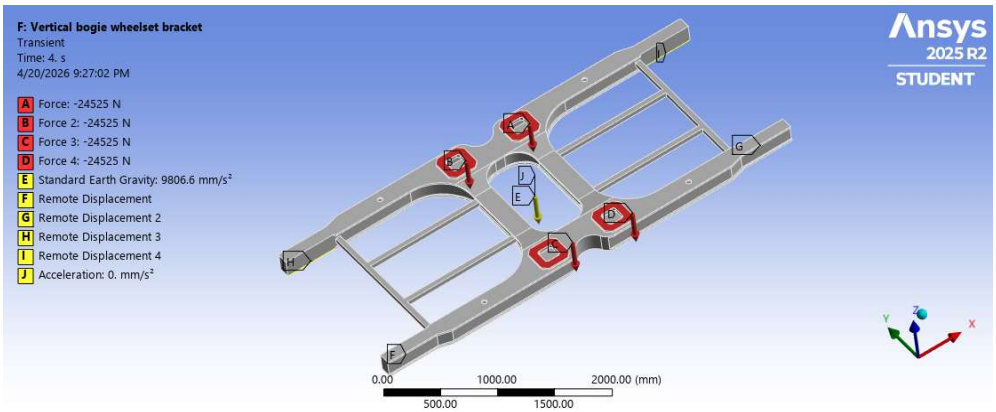

Fig. 7 Remote force area and remote fixed support area

2.5. Basic Principles of Static Structural Analysis

Static structural analysis was conducted under the assumption of linear elastic behavior and static equilibrium conditions [26]. With these assumptions, the stress-strain relationship follows Hooke's law, which is mathematically expressed as

$$\sigma = E\varepsilon \tag{2}$$

where σ is normal stress, E is the modulus of elasticity, and ε is normal strain.

In complex structures such as bogie frames, the stress conditions that occur are multiaxial. Therefore, the equivalent stress criterion was used to evaluate stress concentration in bogie-frame structures [27]. This criterion was also used to compare the relative stress levels σ_v between wheelset bracket configurations, which is formulated as follows:

$$\sigma_v = \sqrt{\frac{1}{2}[(\sigma_1 - \sigma_2)^2 + (\sigma_2 - \sigma_3)^2 + (\sigma_3 - \sigma_1)^2]} \tag{3}$$

where σ_1, σ_2, and σ_3 are the principal stresses, respectively.

In addition to deformation and stress, the structure's stiffness efficiency was evaluated using strain energy analysis. The total strain energy U stored in the structure due to static loading is calculated by:

$$U = \frac{1}{2}\int_{v} \sigma \varepsilon dV \tag{4}$$

where V represents the volume of the structure. Lower strain energy indicates a stiffer structural response and more efficient load distribution. [28]. This study is limited to linear elastic analysis, as the maximum stress obtained remains below the yield strength of SS400 steel. Therefore, material and geometric nonlinearities are not expected to significantly influence the results. Dynamic and impact loading conditions are included in this study to evaluate structural performance under realistic operating scenarios. However, material nonlinearity and geometric nonlinearity are not considered and may be addressed in future work.

3. Finite Element Analysis

This section presents the simulation results and interprets their structural significance for three wheelset bracket configurations. The simulation results are discussed in terms of total deformation, equivalent stress, equivalent elastic strain, and strain energy. A broader comparative interpretation of all configurations is then presented in Section 4.

3.1 Static Load Analysis

This analysis evaluates the structural response of the bogie frame under static loading conditions to establish a baseline for subsequent dynamic and fatigue analyses. The applied load represents the static weight of the train transmitted through the wheelset. The load is applied as vertical concentrated forces on the wheelset bracket, while fixed supports are imposed at the structural boundaries to represent real constraint conditions (based on 2.4. Boundary Conditions and Loading). The simulation results for each wheelset bracket configuration are presented in Figs. 8, 9, and 10.

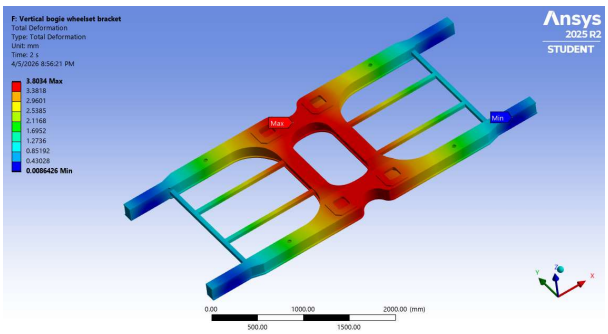

(a) Total deformation vertical wheelset bracket

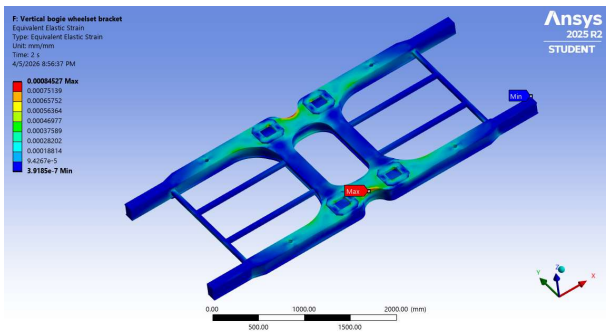

(b) Equivalent elastic strain vertical wheelset bracket

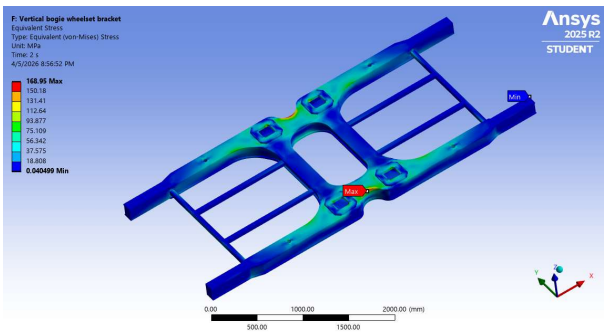

(c) Equivalent stress vertical wheelset bracket

Fig. 8 Simulation results of the vertical wheelset bracket configuration

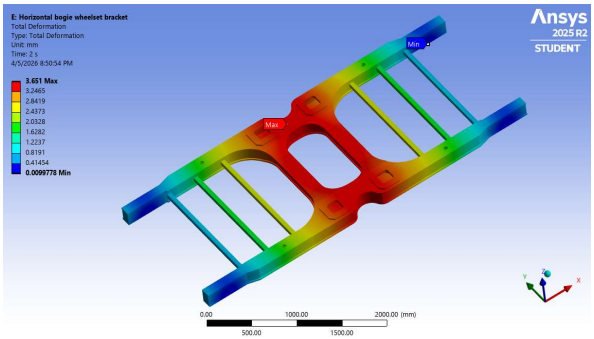

(a) Total deformation horizontal wheelset bracket

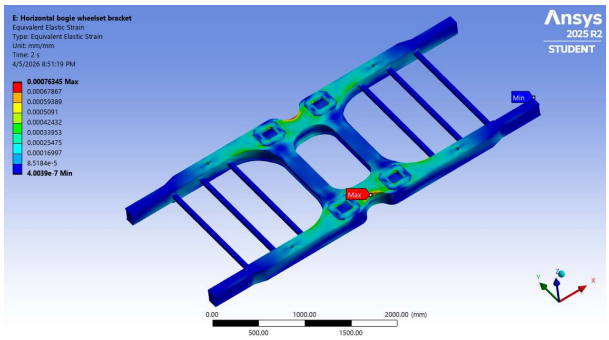

(b) Equivalent elastic strain horizontal wheelset bracket

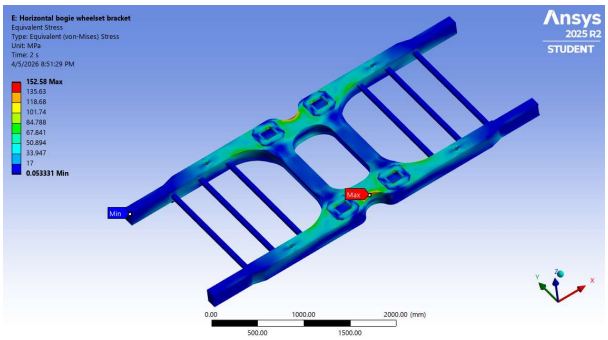

(c) Equivalent stress horizontal wheelset bracket

Fig. 9 Simulation results of the horizontal wheelset bracket configuration

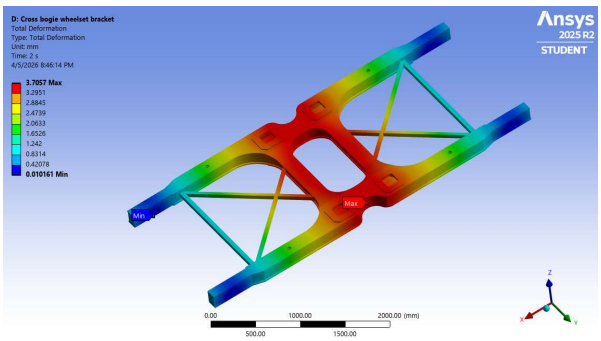

(a) Total deformation cross wheelset bracket

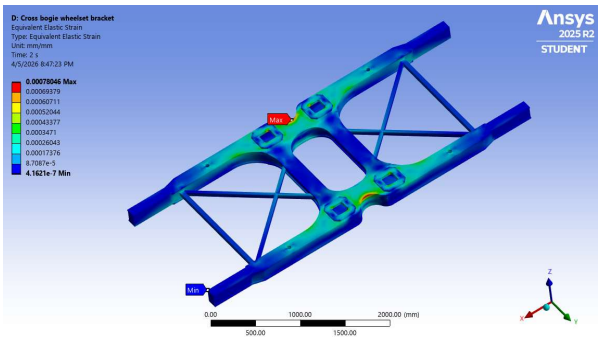

(b) Equivalent elastic strain cross wheelset bracket

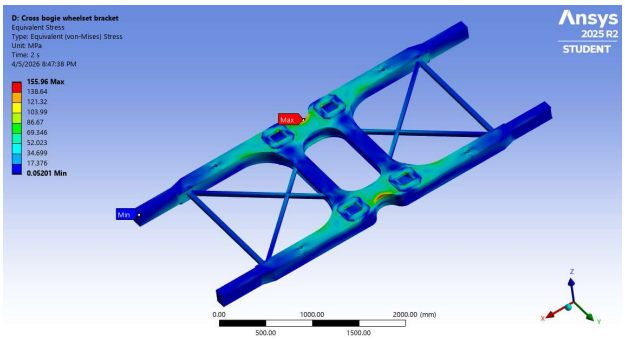

(c) Equivalent stress cross wheelset bracket

Fig. 10 Simulation results of the cross wheelset bracket configuration

A quantitative comparison of the simulation results is provided in Table 3. Each configuration produced different deformation, strain, and stress responses under identical loading conditions. These differences indicate the influence of structural orientation on load transfer behavior. Lower stress and deformation indicate better stiffness and more efficient structural performance. Therefore, a quantitative comparison is required to identify the most effective configuration.

Table 3 Static simulation results

Configuration	Deformation (mm)	Strain	Stress (MPa)
Vertical	3.8034	0.00084527	168.95
Horizontal	3.651	0.00076345	152.58
Cross	3.7057	0.00078046	155.96

The results indicate that the vertical configuration produces the highest stress and deformation, while the horizontal configuration shows the lowest values. This behavior highlights the significant influence of load path orientation on structural performance.

To verify the validity of the results, the stress-strain relationship was evaluated using Eq. (2) by substituting the material properties $(E = 2\times10^5\ MPa)$. The stress verification based on Hooke's law is presented in Table 4. To ensure physical consistency and numerical reliability, the simulated stress values were analytically verified using Hooke's law under elastic material assumptions based on the simulated strain and elastic modulus.

Table 4 Stress verification using Hooke's law

Vertical stress	Horizontal stress	Cross stress
169.05 MPa	152.69 MPa	156.09 MPa

The calculated stress values differ by less than 1% from the simulation results. This indicates good numerical agreement. The stress values range from 152 to 169 MPa. This corresponds to 61-68% of the material yield strength. Therefore, the structure operates within the elastic region [29].

After confirming that the material behaves elastically, the next step is to evaluate the structural safety of each configuration. This is done using the safety factor, which indicates how far the structure is from failure. The safety factor *SF* is defined as

$$SF = \frac{\sigma_y}{\sigma_{\max}} \tag{5}$$

where σ_y is the yield strength (250 MPa) and σ_{max} is the maximum stress obtained from the simulation. The calculated safety factor for each configuration is summarized in Table 5.

Table 5 Safety factor for each configuration under static loading

Configuration	Safety factor
Vertical	1.48
Horizontal	1.64
Cross	1.60

The safety factor values range from 1.48 to 1.64. A safety factor between 1.5 and 2.0 is generally recommended for static structural components. The horizontal and cross configurations satisfy this criterion, indicating adequate structural safety. However, the vertical configuration (SF = 1.48) falls slightly below the recommended lower bound, indicating a marginal safety condition and reduced tolerance to additional loading such as vibration or impact.

To further understand how efficiently the material strength is used, the stress utilization ratio *UR* is evaluated as

$$UR = \frac{\sigma_{\max}}{\sigma_y} \tag{6}$$

where UR is the stress utilization ratio, σ_{max} is the maximum equivalent stress obtained from the simulation, and σ_y is the material yield strength. Values below 1.0 indicate that the structure remains within the elastic region, while values approaching unity indicate more efficient utilization of the material strength. The stress utilization ratio for each configuration is presented in Table 6.

Table 6 Stress utilization ratio under static loading

Configuration	Utilization	Interpretation
Vertical	0.676	Moderate
Horizontal	0.610	Safe
Cross	0.624	Moderate

The vertical configuration shows the highest utilization (0.676), indicating a smaller design margin and higher sensitivity to load variations. In contrast, the horizontal configuration (0.610) is closer to the safe region, indicating better structural efficiency and more reliable performance.

The differences in structural performance are governed by the load transfer mechanism within the frame. The vertical configuration promotes a direct load path, leading to localized stress concentration. In contrast, the horizontal configuration distributes the load more uniformly, resulting in lower stress and improved stiffness. Although the cross configuration adds load paths via bracing, it reduces peak stress less than the horizontal arrangement.

These findings are consistent with previous finite element studies, which show that structural response is strongly influenced by load path and geometric configuration [30]. Configurations that promote direct load transfer tend to produce higher localized stresses. In contrast, configurations that allow load redistribution result in lower stress concentration and improved structural efficiency. A similar trend is observed in the present study. The vertical configuration shows higher stress due to a more direct load path. Meanwhile, the horizontal configuration provides a more uniform load distribution and improved structural performance. This agreement confirms that the numerical model is capable of capturing realistic structural behavior.

In terms of practical application, these results suggest that the horizontal configuration offers a more reliable structural behavior under service conditions. Lower stress levels and a higher safety factor indicate better capacity to withstand operational loads over time. This is directly related to improved durability and reduced maintenance requirements. In contrast, the vertical configuration operates closer to the material limit. It is more sensitive to dynamic loading, vibration, and track irregularities. Therefore, the horizontal configuration offers a more robust and safer design for real-world railway applications.

3.2 Dynamic Load 30% and Cyclic Load Analysis

This analysis evaluates the structural response of the bogie frame under dynamic and cyclic loading conditions using time-history simulation. Unlike static loading, the applied load varies with time due to track irregularities and wheel-rail interaction. This approach allows the evaluation of stress fluctuation, deformation behavior, and fatigue potential under realistic operating conditions.

Dynamic amplification was introduced to account for load fluctuations caused by wheel–rail interaction, track irregularities, and operational vibration. A dynamic amplification factor of ±30% was adopted to represent realistic variations in the wheel load during service. Accordingly, the maximum dynamic load $F_{\max}$ and minimum dynamic load $F_{\min}$ are calculated from the static wheel load F_s, where F_s represents the static wheel load applied to each wheelset bracket location, using

$$F_{\max} = F_s(1+0.3) \tag{7}$$

$$F_{\min} = F_s(1-0.3) \tag{8}$$

where 0.3 is the amplification factor which represents a ±30% variation in the applied load, consistent with operational railway conditions reported in EN 1991-2 and UIC recommendations. Using the static wheel load of $F_s = 24.525$kN as the reference condition, this variation gives $F_{\max} = 31.883$kN and $F_{\min} = 17.167$kN. These values are therefore adopted as the upper and lower bounds of the cyclic loading condition, respectively, to represent load fluctuations during operation. The cyclic load amplitude F_a is subsequently calculated by

$$F_a = \frac{F_{\max} - F_{\min}}{2} = \frac{31.883 - 17.167}{2} = 7.358N \tag{9}$$

where F_a represents the magnitude of cyclic load variation about the mean load. The mean load corresponds to the static wheel load, while the amplitude represents the dynamic fluctuation during operation. These parameters were subsequently applied to define the piecewise cyclic loading in the transient structural analysis. Compared with an idealized sinusoidal excitation, the adopted loading pattern more closely represents the fluctuating wheel loads experienced under actual railway operating conditions. The numerical results obtained from the transient dynamic analysis are summarized in Table 7.

Table 7 Time history results of deformation, strain, and stress under dynamic loading

Time [s]	Vertical			Horizontal			Cross		
	Total deformation	Equivalent elastic strain	Equivalent stress	Total deformation	Equivalent elastic strain	Equivalent stress	Total deformation	Equivalent elastic strain	Equivalent stress
	Maximum [mm]	Maximum [mm/mm]	Maximum [MPa]	Maximum [mm]	Maximum [mm/mm]	Maximum [MPa]	Maximum [mm]	Maximum [mm/mm]	Maximum [MPa]
0.5	4.3456	9.65E-04	192.82	4.1718	8.72E-04	174.17	4.2347	8.91E-04	178.04
1	4.8994	1.09E-03	217.14	4.7033	9.82E-04	196.16	4.7748	1.00E-03	200.53
1.5	3.7978	8.44E-04	168.7	3.6459	7.62E-04	152.36	3.7004	7.79E-04	155.74
2	2.7269	6.07E-04	121.38	2.6174	5.48E-04	109.58	2.6559	5.60E-04	112
2.5	3.7965	8.44E-04	168.64	3.6447	7.62E-04	152.32	3.6992	7.79E-04	155.69
3	4.902	1.09E-03	217.26	4.7058	9.82E-04	196.26	4.7773	1.00E-03	200.63
3.5	3.7967	8.44E-04	168.65	3.6449	7.62E-04	152.32	3.6994	7.79E-04	155.7
4	2.7268	6.07E-04	121.37	2.6173	5.48E-04	109.58	2.6558	5.60E-04	111.99
4.5	3.2557	7.24E-04	144.77	3.1255	6.54E-04	130.74	3.1718	6.69E-04	133.63
5	3.807	8.46E-04	169.1	3.6543	7.64E-04	152.71	3.7091	7.81E-04	156.1
5.5	4.343	9.64E-04	192.71	4.1694	8.71E-04	174.07	4.2323	8.90E-04	177.94
6	4.8997	1.09E-03	217.16	4.7037	9.82E-04	196.17	4.7751	1.00E-03	200.54
6.5	3.7993	8.44E-04	168.76	3.6472	7.63E-04	152.42	3.7018	7.80E-04	155.8
7	2.7242	6.07E-04	121.26	2.615	5.48E-04	109.48	2.6533	5.60E-04	111.89
7.5	3.7999	8.45E-04	168.79	3.6478	7.63E-04	152.45	3.7025	7.80E-04	155.83
8	4.8982	1.09E-03	217.09	4.7023	9.81E-04	196.11	4.7737	1.00E-03	200.48
8.5	4.3455	9.65E-04	192.81	4.1717	8.71E-04	174.16	4.2346	8.91E-04	178.04
9	3.8038	8.45E-04	168.96	3.6514	7.64E-04	152.59	3.7061	7.81E-04	155.98
9.5	3.8012	8.45E-04	168.85	3.649	7.63E-04	152.49	3.7037	7.80E-04	155.88
10	3.8034	8.45E-04	168.94	3.651	7.63E-04	152.58	3.7057	7.80E-04	155.96

The time-history results show a periodic loading pattern representing cyclic behavior. The structure experiences alternating loading and unloading phases, resulting in continuous stress fluctuation. The obtained response indicates a repeated fluctuation pattern throughout the loading duration. This behavior reflects alternating loading and unloading conditions within

the structure. The stress continuously changes during each loading cycle under dynamic excitation. Such cyclic loading is strongly associated with fatigue damage accumulation.

Based on the observed cyclic response, the mean stress σ_m and the stress amplitiude σ_a can be calculated by

$$\sigma_m = \frac{\sigma_{\max} + \sigma_{\min}}{2} \tag{10}$$

$$\sigma_a = \frac{\sigma_{\max} - \sigma_{\min}}{2} \tag{11}$$

where the maximum stress value σ_{max} and minimum stress value σ_{min} are used to characterize the stress variation under dynamic loading. These parameters are required for fatigue assessment using the Goodman criterion. The resulting stress parameters are presented in Table 8.

Table 8 Dynamic stress parameters

Configuration	Mean stress (MPa)	Alternating stress (MPa)
Vertical	169.26	48.00
Horizontal	152.87	43.39
Cross	156.26	44.37

The vertical configuration clearly exhibits the largest stress amplitude. This indicates a wider stress range during each loading cycle. In fatigue mechanics, this is directly associated with accelerated crack initiation. The horizontal configuration shows a lower amplitude, indicating a more stable stress response under fluctuating loads. The cross configuration lies between the two cases. This suggests that added bracing redistributes load but does not significantly reduce peak stress variation.

Table 9 Stress utilization under dynamic loading

Configuration	Utilization	Interpretation
Vertical	0.869	Critical
Horizontal	0.785	Moderate
Cross	0.802	Near-critical

To further assess structural safety, the peak stress is compared against the material yield strength through the utilization ratio. The stress utilization under dynamic loading is summarized in Table 9. The peak stress values are normalized relative to the material yield strength. This approach provides a clearer indication of the remaining structural safety margin. Higher utilization values indicate configurations operating closer to the yield condition.

The vertical configuration reaches about 87% of yield strength. Minor load increases could push it toward yielding. In contrast, the horizontal configuration remains within the moderate zone, indicating a more comfortable safety margin. The cross configuration approaches the critical boundary, suggesting that its performance is improved over the vertical case but remains suboptimal.

To verify that the material remains within the elastic domain, the yield strain ε_y represents the elastic strain limit before the onset of plastic deformation and can be calculated by

$$\varepsilon_y = \frac{\sigma_y}{E} = 0.00125 \tag{12}$$

where σ_y is the yield strength of the material, and E is Young's modulus. The yield strain represents the maximum strain that can be sustained before the onset of plastic deformation. Under dynamic loading, excessive strain may indicate the onset of

permanent deformation. Comparing the obtained strain with the elastic limit helps assess structural reliability. This evaluation is important for identifying configurations approaching plastic behavior. Lower strain ratios indicate better elastic stability during fluctuating loading conditions. The strain evaluation results are shown in Table 10.

Table 10 Strain evaluation under dynamic loading

Configuration	Strain Ratio	Interpretation
Vertical	0.872	Near plastic
Horizontal	0.786	Safe
Cross	0.80	Moderate

A comparison of these values shows that the vertical configuration approaches 87% of the elastic strain limit. In material mechanics, strain levels above approximately 0.8 ε_y indicate a reduced margin before the onset of plastic deformation. The horizontal configuration remains below this threshold, indicating a more reliable elastic response. Meanwhile, the cross configuration sits near the boundary, reflecting moderate performance with a tendency toward higher strain levels.

The deformation behavior is then examined to evaluate the structural stiffness under dynamic conditions, and the percentage increase ($\Delta\delta$) can be calculated by

$$\Lambda\delta = \frac{\delta_d - \delta_s}{\delta_s} \times 100\% \tag{13}$$

where δ_d is the maximum deformation obtained under dynamic loading conditions (mm), and δ_s is the maximum deformation obtained under static loading conditions. This parameter quantifies the effect of dynamic loading on structural stiffness. Higher deformation indicates lower structural rigidity and greater flexibility during load fluctuations. Excessive deformation may amplify vibration levels and reduce structural stability during operation. Therefore, deformation comparison is necessary to evaluate stiffness performance and operational reliability. The deformation comparison is shown in Table 11.

Table 11 Deformation comparison under dynamic loading

Configuration	Maximum deformation (mm)	Increase (%)
Vertical	4.90	28.9
Horizontal	4.70	28.8
Cross	4.78	28.9

It can be observed that the deformation increases by nearly 29% compared to the static condition. Such an increase indicates a noticeable reduction in effective stiffness when the structure is subjected to dynamic loading. Higher deformation at the same load indicates greater flexibility, which may amplify vibration and reduce stability. The slightly higher deformation in the vertical configuration further reinforces its less efficient load transfer mechanism.

To assess the fatigue performance under repeated loading, the Goodman criterion represents the fatigue safety condition under cyclic loading and can be evaluated by

$$\frac{\sigma_a}{\sigma_e} + \frac{\sigma_m}{\sigma_u} < 1 \tag{14}$$

where σ_a is the stress amplitude, σ_e is the endurance limit of the material, σ_m is the mean stress, and σ_u is the ultimate tensile strength of the material. According to the Goodman criterion, values below unity indicate safe operation under cyclic loading conditions.

Repeated stress fluctuation can gradually initiate microcracks within the material structure. Fatigue failure may occur even when the stress remains below the yield strength. Therefore, fatigue assessment becomes essential under cyclic loading conditions. The Goodman criterion combines mean stress and alternating stress into a single parameter. This method is widely

used for evaluating fatigue resistance in engineering structures. Lower Goodman values indicate better resistance against cyclic stress damage. The fatigue evaluation results based on the Goodman criterion are presented in Table 12.

Table 12 Fatigue evaluation based on Goodman criterion under dynamic loading

Configuration	Goodman	Interpretation
Vertical	0.577	Safe
Horizontal	0.521	Safe
Cross	0.533	Safe

All configurations satisfy the fatigue criterion since the computed values remain below unity. However, the vertical configuration produces the highest Goodman value, indicating the smallest margin against fatigue failure. This suggests that under prolonged cyclic loading, it is more susceptible to damage accumulation. The horizontal configuration, which yields the lowest value, demonstrates better resistance to cyclic stress and is therefore expected to have a longer fatigue life. The cross configuration provides intermediate performance, confirming that additional bracing improves load redistribution but does not significantly reduce fatigue-critical stresses.

The observed performance differences can be attributed to the load-transfer mechanism in each configuration. In the vertical arrangement, the load follows a relatively direct path, which tends to concentrate stress in localized regions. From an application standpoint, these findings highlight the importance of considering dynamic effects in structural design. A configuration that appears adequate under static loading may exhibit critical behavior when subjected to fluctuating loads. The vertical configuration operates near material limits, making it more vulnerable to vibration and track irregularities. This may accelerate fatigue damage and increase maintenance demands. In contrast, the horizontal configuration shows a more balanced response. It has lower stress, smaller deformation, and better fatigue resistance. These features improve durability and reliability, making it more suitable for practical railway applications.

3.3 Impact Load Analysis

This analysis evaluates bogie frame response under impact loads from rail joints and track irregularities. The peak structural response obtained from the impact simulation is summarized in Table 13. Unlike cyclic loading, impact loading is governed by a single dominant peak, making the maximum response the primary parameter for assessing structural safety. In practical railway operation, this condition is critical because sudden load amplification can approach the material limit and directly influence failure risk.

To represent the amplification caused by sudden contact, the impact load F_i represents the amplified wheel load during sudden loading events and can be calculated by

$$F_i = k \cdot F_s \tag{15}$$

where k is the impact amplification factor, and F_s is the static wheel load. The amplification factor accounts for the increase in load caused by sudden wheel–rail interactions and impact events. This amplification reflects realistic railway conditions, where dynamic effects can significantly exceed static loads. According to UIC 776-2, impact factors in the range of 1.2-1.6 are commonly used to represent such conditions. This indicates that structures designed only for static loads may experience critical stress levels under impact events.

Table 13 Peak response

Configuration	Total deformation (mm)	Equivalent elastic strain	Equivalent stress (Mpa)
Vertical	5.231	1.16E-03	231.84
Horizontal	5.020	1.05E-03	209.41
Cross	5.100	1.07E-03	214.21

The vertical configuration exhibits the highest response across all parameters. A stress value of 231.84 MPa corresponds to about 92.7% of the yield strength. This indicates that the structure operates very close to its allowable limit. According to EN 1993-1-1 Eurocode 3, stress levels above 0.8σ_y are considered critical. In real operation, this increases dependence on track condition and inspection quality. The horizontal configuration shows lower stress and deformation values. This indicates a more effective load distribution mechanism. The cross configuration provides moderate improvement but does not significantly reduce peak response.

Table 14 Stress utilization under impact loading

Configuration	Utilization	Interpretation
Vertical	0.927	Critical
Horizontal	0.838	Near-critical
Cross	0.857	Critical

This normalization provides a clear measure of how close the structure operates to its allowable limit. The stress utilization under impact loading is presented in Table 14. Stress normalization is used to evaluate structural loading severity under impact conditions. The obtained ratio indicates the proximity to the allowable material stress limit. Higher utilization values correspond to reduced safety margins during sudden loading. This parameter helps identify structures vulnerable to impact-induced failure.

The vertical configuration reaches 92.7% of the yield strength, indicating that the structure operates very close to its allowable limit. The horizontal configuration exhibits a lower utilization value, indicating a more stable stress distribution and a greater tolerance to load variation. This behavior occurs because the load is distributed more evenly across structural members, reducing stress concentration. The cross configuration shows intermediate behavior, where additional load paths partially redistribute the force, but the peak stress remains relatively high.

To evaluate the deformation response, the strain is normalized with respect to the elastic limit. This allows the material behavior to be assessed in terms of its proximity to plastic deformation. The strain evaluation results are shown in Table 15.

Table 15 Strain evaluation under impact loading

Configuration	Strain Ratio	Interpretation
Vertical	0.928	Near plastic
Horizontal	0.84	Moderate
Cross	0.856	Near-critical

The vertical configuration reaches a strain ratio of 0.928, indicating that the deformation state approaches the elastic limit. The horizontal configuration shows a lower strain ratio of 0.84, indicating a more stable deformation response and improved elastic behavior. The cross configuration exhibits intermediate behavior, reflecting partial improvement due to additional load paths. However, localized deformation is still present, indicating that redistribution is not fully effective.

Table 16 Deformation comparison under impact loading

Configuration	Maximum deformation (mm)	Interpretation
Vertical	5.231	Lowest stiffness
Horizontal	5.020	Highest stiffness
Cross	5.100	Moderate

Table 16 shows the summary of deformation comparison. To evaluate structural stiffness under impact loading, stiffness k is used to describe the resistance of the structure to deformation. A higher stiffness indicates greater resistance to displacement, while a lower stiffness indicates greater deformation under the applied load. The relationship between structural stiffness and deformation is expressed as

$$k \propto \frac{1}{\delta} \tag{16}$$

where δ denotes the displacement under impact loading. This inverse relationship indicates that lower displacement corresponds to higher structural stiffness. Therefore, the deformation response can be used to compare the stiffness performance of the three bracket configurations.

The vertical configuration exhibits the largest deformation, reaching 5.231 mm, which indicates reduced structural stiffness under impact loading. This condition increases susceptibility to vibration and local instability, particularly under repeated loading. In practical applications, such behavior may accelerate wear and reduce structural reliability over time. The horizontal configuration shows the lowest deformation, indicating a stiffer response and more effective load transfer. The cross configuration presents an intermediate deformation value. However, the reduction remains limited, suggesting that stiffness enhancement is not significant.

To evaluate the dynamic characteristics of the structure, the equivalent wheel-supported mass m represents the mass associated with the static wheel load and can be calculated by

$$m = \frac{F_s}{g} \tag{17}$$

where g is the gravitational acceleration. The equivalent mass is subsequently used to determine the natural angular frequency of the structure. Using the equivalent mass and structural stiffness, the natural angular frequency ω_n represents the characteristic angular frequency of the structure and can be calculated from

$$\omega_n = \sqrt{\frac{k}{m}} = \sqrt{\frac{g}{\delta}} \tag{18}$$

where k is the structural stiffness, m is the equivalent mass, and δ is the static deformation obtained from the simulation results. The natural frequency f_n represents the characteristic frequency of the structure and can be calculated from the natural angular frequency through the following equation

$$f_n = \frac{\omega_n}{2\pi} \tag{19}$$

where ω_n is the natural angular frequency. The calculated natural frequency is subsequently compared with the operational excitation frequency to evaluate the possibility of resonance. Based on the deformation values obtained from the impact analysis, the calculated natural frequencies for each configuration are presented in Table 17.

As shown in Table 17, the natural frequency of all configurations lies within a narrow range of approximately 6.9 to 7.0 Hz. This indicates that the global stiffness of the structure does not vary significantly between configurations. Since the mass remains constant, the variation in natural frequency is primarily governed by differences in stiffness. The horizontal configuration exhibits the highest frequency, reflecting its higher stiffness, while the vertical configuration shows the lowest value, indicating reduced rigidity.

Table 17 Natural frequency estimation under impact loading

Configuration	Natural angular frequency (rad/s)	Natural frequency (Hz)
Vertical	43.32	6.89
Horizontal	44.25	7.04
Cross	43.85	6.98

When compared with the excitation frequency associated with the impact event, which occurs over a time scale of approximately 1 s (≈1 Hz), it is evident that the system operates well below its natural frequency. This condition can be expressed as

The potential for resonance is evaluated by comparing the operational excitation frequency with the natural frequency of the structure. A sufficiently large separation between these frequencies indicates a lower likelihood of resonance during operation and is expressed as

$$f_e \ll f_n \tag{20}$$

where f_e is the operational excitation frequency. This criterion indicates that the excitation frequency is substantially lower than the natural frequency, thereby reducing the likelihood of resonance during operation.

To assess the dynamic response, the structural behavior is evaluated in terms of acceleration. The acceleration response a describes the rate of change in structural motion during impact loading and is obtained from the displacement history through its second derivative with respect to time as

$$a = \frac{d^2u}{dt^2} \tag{21}$$

where u denotes the structural displacement, and t represents time. The resulting acceleration is subsequently used to determine the inertial force generated by the equivalent mass during the impact event. Based on Newton's second law, the applied impact force F represents the inertial force generated by the equivalent mass in response to the acceleration and is determined as

$$F = m \cdot a \tag{22}$$

where a is the acceleration response. This relationship establishes the connection between the structural acceleration and the force developed during sudden loading events. The resulting force provides an indication of the inertial response experienced by the structure under impact loading. The calculated acceleration response is presented in Table 18.

Table 18 Acceleration response under impact loading

Configuration	Acceleration (mm/s²)	Interpretation
Vertical	22.231	Highest dynamic response
Horizontal	21.331	Smooth response
Cross	21.634	Moderate

The vertical configuration produces the highest acceleration, indicating a stronger inertial response under impact loading. Based on the relation $F = m \cdot a$, higher acceleration leads to greater internal dynamic forces, which can increase vibration intensity and accelerate material degradation. The horizontal configuration exhibits lower acceleration, indicating a smoother energy transfer and reduced dynamic amplification. The cross configuration shows intermediate behavior, reflecting partial improvement in load redistribution.

To evaluate long-term structural performance, fatigue behavior is considered due to the repetitive nature of impact loading. Even when short-term safety is satisfied, cumulative damage may develop over time. Fatigue evaluation results are summarized in Table 19.

Table 19 Fatigue evaluation under impact loading

Configuration	Goodman	Interpretation
Vertical	0.718	Safe (low margin)
Horizontal	0.65	Safer
Cross	0.67	Moderate

All configurations satisfy the fatigue criterion, indicating that fatigue failure is not expected under the given loading condition. However, the vertical configuration exhibits the highest Goodman value, indicating a reduced fatigue margin compared to the other configurations. At this level, the structure remains safe but becomes more susceptible to long-term damage accumulation. The horizontal configuration shows the lowest Goodman value, indicating better resistance to cyclic stress and improved durability. The cross configuration provides moderate improvement, although its effect on fatigue performance remains limited.

The differences in structural response under impact loading are governed by the load transfer mechanism within each configuration. In the vertical arrangement, loads follow a direct path along primary members. This promotes localized stress concentration and limits energy redistribution. This results in higher stress, larger deformation, and increased dynamic response. In contrast, the horizontal configuration distributes the load across multiple structural members, reducing stress concentration and improving stiffness. This leads to a more stable response with lower deformation and reduced dynamic amplification. The cross configuration adds load paths, but its effectiveness is limited by the dominant primary load direction.

Impact loading represents one of the most critical conditions in railway operation. The vertical configuration operates near the material limit and is more sensitive to dynamic excitation. This increases the risk of fatigue damage and structural degradation. Conversely, the horizontal configuration shows a more balanced response, with lower stress, reduced deformation, and better resistance to impact damage. These features improve durability and reliability, making it the most suitable for real-world railway applications.

4. Conclusion

This study presented a comparative finite element analysis of a railway bogie frame with three wheelset bracket orientations: vertical, horizontal, and cross. All configurations were evaluated under identical geometry, material properties, boundary conditions, and loading conditions. Structural performance was assessed using deformation, stress, strain, fatigue behavior. While dynamic characteristics was assessed under static, dynamic, cyclic, and impact loading conditions. Based on the results, the following conclusions are drawn:

(1) The wheelset bracket orientation significantly affects structural behavior through load-transfer characteristics and stress distribution. Under static loading, the vertical configuration produced the highest stress (168.95 MPa) and deformation (3.803 mm), while the horizontal configuration showed the lowest values (152.58 MPa and 3.651 mm), indicating better stiffness and load distribution.

(2) The horizontal configuration demonstrated the best structural performance under all loading conditions. It achieved the highest safety factor (1.64), lowest stress utilization (0.610), and lower dynamic stress amplitude (43.39 MPa), indicating improved elastic stability and fatigue resistance.

(3) The vertical configuration generated a more direct load path, causing higher localized stress and deformation. In contrast, the horizontal configuration distributes loads more uniformly, reducing peak stress and improving structural rigidity. The cross configuration provided intermediate performance.

(4) Under dynamic and impact loading, the vertical configuration showed the most critical response. Peak stresses reached 217 MPa during cyclic loading and 231.84 MPa under impact loading, corresponding to 92.7% of the material yield strength. Meanwhile, the horizontal configuration maintained lower stress and deformation, indicating better resistance to fatigue and impact effects.

(5) Dynamic loading increased deformation by approximately 29% compared to static loading, indicating reduced effective stiffness under fluctuating loads. The natural frequency ranged from 6.89 to 7.04 Hz, remaining well above the operational excitation frequency, thereby minimizing resonance potential.

This study is limited by the use of linear elastic material assumptions and simplified loading conditions. Material nonlinearity, cumulative fatigue damage, and experimental validation were not included. Future work should incorporate nonlinear material models, fatigue-life prediction, realistic track excitation, and experimental validation to improve model reliability and practical applicability.

Conflicts of Interest

The authors declare no conflict of interest.

References

[1] Z. KNikšić D. Pavković, M. Cipek, M. Trstenjak, T. J. Mlinarić, and M. Nikšić, "An Overview of Current Challenges and Emerging Technologies to Facilitate Increased Energy Efficiency, Safety, and Sustainability of Railway Transport," Future Internet, vol. 15, no. 11, article no. 347, 2023.

[2] C. Bragança, E. F. Souza, D. Ribeiro, A. Meixedo, T. N. Bittencourt, and H. Carvalho "Drive-by Methodologies Applied to Railway Infrastructure Subsystems: A Literature Review-Part II: Track and Vehicle," Applied Sciences, vol. 13, no. 12, article no. 6982, 2023.

[3] M. M. Islam, M. S. Hossain, M. R. Islam, and M. A. Hossain, "Improving Reliability and Stability of Power Systems: A Comprehensive Review on the Role of Energy Storage Systems to Enhance Flexibility," IEEE Access, vol. 12, pp. 152738-152765, 2024.

[4] Y. Wu and Z. Ren, "Fatigue Damage Assessment of a Metro Vehicle Bogie Frame Based on Measured Field Load," Machines, vol. 13, no. 4, article no. 306, 2025.

[5] G. Papaioannou, C. Shen, M. Rothhämel, and R. Happee, "Occupants Comfort: What About Human Body Dynamics in Road and Rail Vehicles?," Vehicle Mechanics and Mobility, vol. 63, no. 7, pp. 1242-1245, 2025.

[6] K. Holenko, O. Dykha, E. Koda, I. Kernytskyy, O. Horbay, Y. Royko, et al., "Structure and Strength Optimization of the Bogdan ERCV27 Electric Garbage Truck Spatial Frame Under Static Loading," Applied Sciences, vol. 14, no. 23, article no. 11012, 2024.

[7] M. Xie, Y. Wei, Q. Xin, L. Li, and Y. He, "Fatigue Resistance of Fillet Welds of Traction Rod Brackets on a Locomotive Bogie Based on International Union of Railways Standards and Improvement Measures Adopted," Applied Sciences, vol. 13, no. 9, article no. 5494, 2023.

[8] T. J. Dang, Z. Liu, P. Masarati, M. Morandini, L. J. Ma, and X. W. Zhou, "Multibody Dynamics Modeling and Simulation of Supersonic Flexible Rocket Sled-Track Systems," American Institute of Aeronautics and Astronautics Journal, vol. 63, no. 7, pp. 2847-2869, 2025.

[9] A. Cascino, E. Meli, and A. Rindi, "Development of a Design Procedure Combining Topological Optimization and a Multibody Environment: Application to a Tram Motor Bogie Frame," Vehicles, vol. 6, no. 4, pp. 1843-1856, 2024.

[10] A. Ortiz-Marqués, P. Caldevilla, E. Goldmann, M. Safuta, M. Fernández-Raga, and M. Górski, "Porosity and Permeability in Construction Materials as Key Parameters for Their Durability and Performance: A Review," Buildings, vol. 15, no. 18, article no. 3422, 2025.

[11] I. A. Najar, R. Ahmadi, A. G. Amuda, R. Mourad, N. El Bendary, I. Ismail, et al., "Advancing Soil-Structure Interaction (SSI): A Comprehensive Review of Current Practices, Challenges, and Future Directions," Journal of Infrastructure Preservation and Resilience, vol. 6, article no. 5, 2025.

[12] S. K. Shil, "Petroleum Storage Tank Design and Inspection Using Finite Element Analysis Model for Ensuring," Review of Applied Science and Technology, vol. 3, no. 4, pp. 94-127, 2024.

[13] F. Guo, S. Wu, J. Liu, X. Wu, and W. Zhang, "An Innovative Stepwise Time-Domain Fatigue Methodology to Integrate Damage Tolerance into System Dynamics," Vehicle Mechanics and Mobility, vol. 61, no. 2, pp. 550-572, 2023.

[14] A. Yusufov, O. Khamidov, and N. Zayniddinov, "Prediction of the Stress - Strain State of the Bogie Frames of Shunting Locomotives using the Finite Element Method," E3S Web of Conferences, vol. 401, article no. 03041, 2023.

[15] C. Pany, "Vibration Analysis of Curved Panels and Shell Using Approximate Methods and Determination of Optimum Periodic Angle," Advances in Mechanical and Power Engineering, pp. 354-365, 2023.

[16] K. Shabla and C. Pany, "Finite Element Structural Analysis of Simply Supported Solid and Stiffened Plates: A

Comparative Study," Mechanical Engineering Advances, vol. 3, no. 1, article no. 1405, 2024.

[17] C. Pany, "Cylindrical Shell Pressure Vessel Profile Variation Footprint in Strain Comparison of Test Data with Numerical Analysis," Liquid and Gaseous Energy Resources, vol. 1, no. 2, pp. 91-101, 2021.

[18] M. A. Sayeed and M. A. Shahin, "Dynamic Response Analysis of Ballasted Railway Track–Ground System under Train Moving Loads using 3D Finite Element Numerical Modelling," Transportation Infrastructure Geotechnology, vol. 10, pp. 639-659, 2023.

[19] M. Eghlimi, P. Memarzadeh, E. I. Z. Abadi, and P. Javadi, "An Innovative Two-Level Yielding Knee-Braced Frame with Deformation-Controlled Ring Damper," Case Studies in Construction Materials, vol. 21, article no. e03856, 2024.

[20] L. Gao, Y. Zhang, Y. Liu, Z. Wang, and X. Ji, "Study on the Cracking Behavior of Asphalt Mixture by Discrete Element Modeling with Real Aggregate Morphology," Construction and Building Materials, vol. 368, article no. 130406, 2023.

[21] M. J. Hörmann, "Topology Optimization of an Electric Powertrain Suspension Bracket," Master degree, Department of Engineering Mechanics, KTH Royal Institute of Technology, Stockholm, Sweeden, 2023.

[22] K. Yelemessov, D. Baskanbayeva, N. V Martyushev, V. Y. Skeeba, V. E. Gozbenko, and A. I. Karlina, "Change in the Properties of Rail Steels during Operation and Reutilization of Rails," Metals, vol. 13, no. 6, article no. 1043, 2023.

[23] Y. Huang and J. Jiang, "A Critical Review of von Mises Criterion for Compatible Deformation of Polycrystalline Materials," Crystals, vol. 13, no. 2, article no. 244, 2023.

[24] R. G. Shang, S. Y. Xie, L. Q. Liao, G. Z. Qin, X. Y. Zhu, Z. H. Wang, et al., "Development, Validation, and Biomechanical Evaluation of a High-Fidelity Finite Element Model of the Forearm Musculoskeletal System," BMC Musculoskeletal Disorders, vol. 27, article no. 223, 2026.

[25] T. A. Burkhart, D. M. Andrews, and C. E. Dunning, "Finite Element Modeling Mesh Quality, Energy Balance and Validation Methods: A Review with Recommendations Associated with the Modeling of Bone Tissue," Journal of Biomechanics, vol. 46, no. 9, pp. 1477-1488, 2013.

[26] D. Oldoini, S. G. Barbieri, G. Devito, M. Giacopini, and M. Galea, "Effects of an Optimized Adhesive Distribution on Stresses and Strains in the Rotor and Magnets of a Surface Permanent-Magnet Synchronous Electric Motor," Applied Sciences, vol. 15, no. 24, article no. 13179, 2025.

[27] X. Liu, Q. Wang, Y. Wang, and Q. Dong, "Review of Calibration Strategies for Discrete Element Model in Quasi-Static Elastic Deformation," Scientific Reports, vol. 13, no. 1, article no. 13264, 2023.

[28] S. Raghavendra, M. Dallago, F. Zanini, S. Carmignato, F. Berto, and M. Benedetti, "A Probabilistic Average Strain Energy Density Approach to Assess the Fatigue Strength of Additively Manufactured Cellular Lattice Materials," International Journal of Fatigue, vol. 172, article no. 107601, 2023.

[29] C. K. Park, C. T. Wu, and C. D. Kan, "On the Analysis of Dispersion Property and stable time step in Meshfree Method using the Generalized Meshfree Approximation," Finite Elements in Analysis and Design, vol. 47, no. 7, pp. 683-697, 2011.

[30] Ö. Kırmalı, N. Türker, T. Akar, and B. Yılmaz, "Finite Element Analysis of Stress Distribution in Autotransplanted Molars," Journal of Dentistry, vol. 119, article no. 104082, 2022.

Copyright© by the authors. Licensee TAETI, Taiwan. This article is an open-access article distributed under the terms and conditions of the Creative Commons Attribution (CC BY-NC) license (https://creativecommons.org/licenses/by-nc/4.0/).